

Influence of silver electrochemically deposited onto zinc oxide seed nanoparticles on the photoelectrochemical performance of zinc oxide nanorod films

Alejandro Aranda¹, Richard Landers², Patricio Carnelli³ ,
Roberto Candal³, Hugo Alarcón¹, and Juan Rodríguez¹

Abstract

The present article examines the synthesis and characterization of zinc oxide nanorods grown on zinc oxide and silver nanoparticle seeds. Zinc oxide seeds were electrodeposited on a support of fluorine-doped tin oxide glass and heat-treated at 380°C. Silver nanoparticles were then deposited on this substrate, which was heat-treated at 160°C. Their presence was confirmed using ultraviolet–visible spectroscopy, by observing an absorption peak around 400 nm, corresponding to surface plasmon resonance. Growth of zinc oxide nanorods was achieved in a chemical bath at 90°C. The obtained films were analyzed by cyclic voltammetry, X-ray diffraction, and scanning electron microscopy. They consisted of zinc oxide with a Wurtzite-type crystal structure, arranged as nanorods of 50 nm. X-ray photoelectron spectroscopy exhibits peaks attributed to silver (0) and to the formation of silver oxide on the silver nanoparticle surface. In addition, two types of oxygen (O 1 s) were observed: oxygen from the crystalline network (O²⁻) and chemisorbed oxygen (–OH), for the seed and the nanorod films, respectively. The nanorods grown on zinc oxide seeds with silver deposits had a round shape and greater photoactivity than those grown without silver. This difference is attributed to the additional reflection that silver provides to the light reaching the film, thereby increasing the photogeneration from the charge carriers.

Keywords

Electrodeposition, zinc oxide, silver, nanoparticles, nanorods, films, photocurrent

Date received: 27 August 2018; accepted: 7 March 2019

Topic: Low Dimensional Semiconductor and Graphene-Like Nanostructures

Topic Editor: Paola Prete

Associate Editor: Nico Lovergine

Introduction

The optical bandwidth of semiconductors lies within the ultraviolet (UV)–visible (UV-Vis) range.¹ When synthesized as thin films, they have been used as optoelectronic² and photovoltaic³ devices, as well as for water purification.^{4,5} The substrates used have included blends of silicon,⁶ glasses,⁷ conductive glasses of fluorine-doped tin oxide (FTO),⁸ among others. Zinc oxide (ZnO) films have an optical bandwidth of 3.18–3.37 eV,^{2,9} which allows them to absorb UV-A radiation, a property of interest in photovoltaic applications. Within their morphologies, there

¹Center for the Development of Advanced Materials and Nanotechnology, Universidad Nacional de Ingeniería, Lima, Peru

²Applied Physics Department, Universidade Estadual de Campinas, Campinas, Brazil

³Instituto de Investigación e Ingeniería Ambiental, CONICET, Escuela de Ciencia y Tecnología, Universidad Nacional de San Martín, Buenos Aires, Argentina

Corresponding author:

Juan Rodríguez, Center for the Development of Advanced Materials and Nanotechnology, Universidad Nacional de Ingeniería, Av. Tupac Amaru 210, Rimac, Lima 25, Peru.

Email: jrodriguez@uni.edu.pe



are vertically aligned nanostructures that have been exhaustively used as electron transport materials in photovoltaic cells. Nanorods, nanotubes, or nanowires, high surface area nanostructures, increase the absorption of photons.¹⁰ In these materials, the bandgap variations would also improve the absorption of lower energy photons.¹¹ The development of ZnO films is very attractive for these applications, as the synthesis process can modify their structure and morphology. Within the methods of nanorods synthesis, we can find carbothermal evaporation,¹² seed-layer-assisted solvothermal method,¹³ hydrothermal method,¹⁴ and chemical bath deposition.¹⁵ When using the chemical bath deposition process, the substrate is first covered by a thin seed layer of the material to be deposited. This layer can be prepared by the sol-gel method,^{16,17} which makes it possible to obtain a variety of morphologies for the material to be grown on the substrate. This seeding step usually takes place between 70°C and 90°C in an alkaline solution of zinc nitrate ($\text{Zn}(\text{NO}_3)_2 \cdot 6\text{H}_2\text{O}$)¹⁷ and zinc acetate ($\text{Zn}(\text{CH}_3\text{COO})_2 \cdot 2\text{H}_2\text{O}$),¹⁶ which modifies the growth pattern of the films.

A versatile and easy to implement process developed in the last few years is the electrochemical method,⁸ which allows adjusting parameters for modifying the growth characteristics, and does not require high temperatures like other methods.¹⁸ It consists in obtaining on the electrode surface the reduction of OH^- producing species, which react with the Zn^{2+} ions in solution. This leads to the deposition and growth of thin layers on the FTO^{8,17} or indium tin oxide conducting electrode. This usually takes place at temperatures between 60°C and 80°C^{8,18} with salts like ($\text{Zn}(\text{NO}_3)_2 \cdot 6\text{H}_2\text{O}$)⁸ or ZnCl_2 .¹⁹

To improve the ZnO structure and avoid carrier recombination, hybrid materials have been developed by combining ZnO with p-type semiconductors, such as copper oxide,¹⁹ or by doping with metallic ions, such as Ni,⁹ Fe,¹⁸ or Co,^{20,21} mainly to improve ferromagnetic properties and to increase the optical absorption range. The addition of metallic nanoparticles in ZnO nanorods improves the electronic and chemical effect of the surface of the nanorods, improving their applications as a sensor²²; these induce an effective electron-hole separation on the ZnO particles.²³ Recent studies have shown that metal nanoparticles can be used to improve the semiconducting properties of ZnO films, by generating surface plasmon resonance. Through the adjustment of size and composition of the nanoparticles,²⁴ this phenomenon can cause the absorption of sunlight in the visible range and improve the photochemical response. Among the methods of metal nanoparticle synthesis, we can find radio frequency sputtering technique,²⁴ laser ablation,²³ chemical reduction,²² photodeposition,¹⁶ and electrodeposition,²⁵ the latter being a practical method which uses not expensive equipment or reagents, in which the morphology of the films can be modified.

This work is focused on the production of silver (Ag) nanoparticle seeds by electrodeposition method to obtain

ZnO nanorods, in order to reduce the recombination process and improve its photocatalytic effect.

Experimental details

Preparation of ZnO seeds

ZnO seeds were electrodeposited²⁶ on a 5-cm² FTO glass conductor washed in 5% nitric acid and ultrapure water. A 0.1-M zinc acetate dehydrate solution with a 0.1-M sodium nitrate (NaNO_3) as a supporting electrolyte in order to improve the electrolytic medium conductivity and a polyvinylpyrrolidone (PVP) with a final concentration of 4 g/L for size control of ZnO seeds were used. This solution was introduced in an electrochemical cell equipped with an Ag/silver chloride (AgCl) reference electrode, a platinum counter electrode, and the FTO sample as the working electrode. The electrochemical process took place at 70°C.

Cyclic voltammetry was performed with a potential window between -1.5 V and -0.5 V, and a reduction peak was observed at -1.1 V, corresponding to ZnO electrodeposition, as shown in Figure 1(a); the O_2 was not removed from the solution, because O_2 is needed for the oxide formation process on the FTO surface. The actual electrodeposition was carried out by chronoamperometry, fixing the potential at -1.1 V for 240 s, under dark conditions. Finally, the samples were rinsed in ultrapure water and heat-treated for 2 h at 380°C.

Preparation of Ag nanoparticles

Ag nanoparticles²⁷ were electrodeposited from a 2×10^{-4} M silver nitrate solution, which contained as well 4 g/l of PVP as surfactant, 0.01 M of sodium citrate ($\text{Na}_3\text{C}_3\text{H}_5\text{O}(\text{COO})_3$), and 0.1 M of NaNO_3 as supporting electrolyte. The operation took place at 60°C using an Ag/AgCl reference electrode, a platinum wire as counter electrode, and the sample of FTO glass covered with previously deposited nanoporous ZnO seeds as working electrode. A cyclic voltammogram with a potential window between -0.95 V and 0 V gave an Ag reduction peak at -0.4 V, as it can be seen in Figure 1(b). Ag was electrodeposited by chronoamperometry at -0.4 V, for periods varying from 100 s to 400 s. Finally, the sample was rinsed in ultrapure water and heat-treated at 160°C for 30 min.

ZnO nanorods growth on Ag/ZnO seeds

ZnO nanorods growth²⁸ was performed in a chemical bath solution containing 0.8 M sodium hydroxide, to which a 0.08 M solution of $\text{Zn}(\text{NO}_3)_2 \cdot 4\text{H}_2\text{O}$ was added. This solution was stirred for 3 h. After that time, $\text{Zn}(\text{OH})_{2(s)}$ was removed by filtration and the filtrate was used as a growth solution, in which FTO glass samples with Ag/ZnO seeds were immersed for 75 min at 90°C. Finally, the samples were left to dry at room temperature.

The whole procedure is presented in Figure 2.

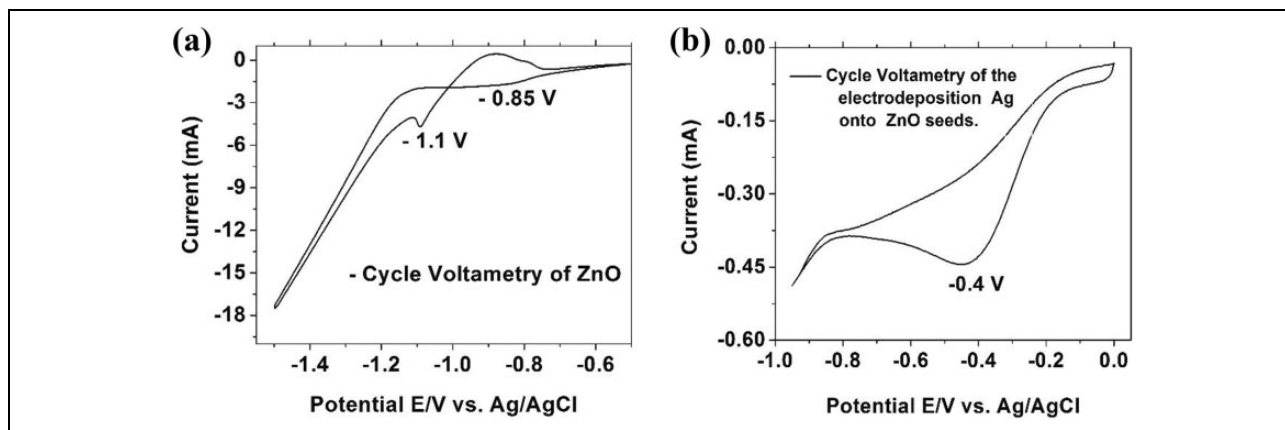


Figure 1. Electrodeposition using cyclic voltammetry at (50 mV/s) onto FTO: (a) ZnO seeds and (b) Ag electrodeposition onto ZnO seeds. FTO: fluorine-doped tin oxide; ZnO: zinc oxide; Ag: silver.

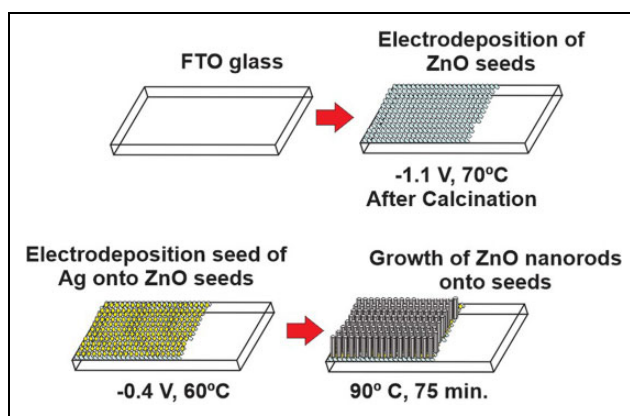


Figure 2. General outline of film growth.

Photoelectrochemical characterization

The films were analyzed by cyclic voltammetry with a Princeton Applied Research model 263A potentiostat/galvanostat, in a 1 mM solution of NaNO_3 at a scan rate of 50 mV/s using a potential range of -1.0 V to 1.0 V. Twenty cycles were used to reach stability, and the results presented here are those of the last cycle. When the analysis was done with light, the film was illuminated with a Westinghouse (13 W) lamp, in which an increase in the photocurrent was observed, due to the charge carrier's separation effect of light on the surface of the films (Figure 3).

Characterization of the films

The Ag/ZnO nanorod films were examined by X-ray diffraction, with a Philips PANalytical X'PERT MPD diffractometer (Panalytical, Eindhoven, the Netherlands), using copper K_α as a source of radiation ($\lambda = 0.154$ nm). The optical transmittance was measured with a Shimadzu 1800 spectrophotometer (Shimadzu, Kyoto, Japan), with a measuring range between 190 nm and 1100 nm.

The morphological structure of the films was characterized with a Zeiss Supra 40 field emission scanning electron

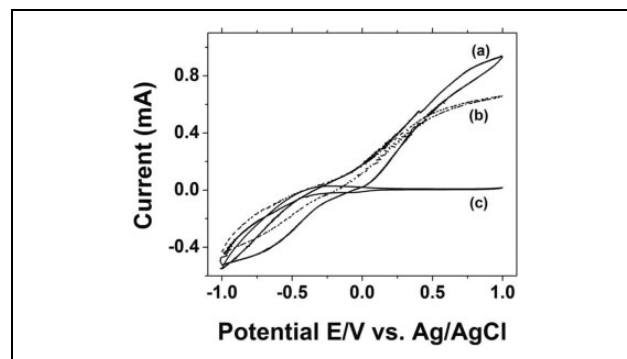
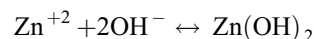


Figure 3. Cyclic voltammetry at 50 mV/s for: (a) ZnO nanorod films onto Ag/ZnO seeds under UV-A illumination, (b) ZnO nanorod films under UV-A illumination, and (c) ZnO nanorods in the dark. ZnO: zinc oxide; Ag: silver; UV: ultraviolet.

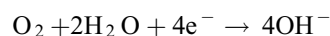
microscope (Carl Zeiss AG, Oberkochen, Germany) (SEM), operating at 3 kV. The chemical species present in the films were identified with a VSW HA-100 X-ray photoelectron spectrophotometer (XPS) spherical analyzer (VSW Atomtech Ltd, Oxfordshire, UK), using an aluminum (Al) anode (Al K_α line, $h\nu = 1486.6$ eV) as the X-ray source.

Results and discussion

The main reaction in the electrodeposition of ZnO is based on the reduction of the precursor of OH^- , for the formation of $\text{Zn}(\text{OH})_2$ according to the equation



In the electrochemical deposition of ZnO, the concentration of OH^- ions at the electrode interface can be controlled by the reduction of precursors, such as O_2 or nitrate ions (NO_3^-). The presence of molecular O_2 in the solution is due to the aerobic conditions under which the process occurs. The electroreduction of O_2 to hydroxide ions is based on the following reaction



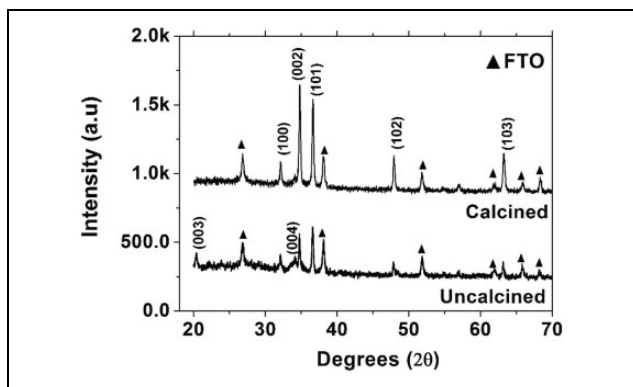
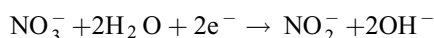


Figure 4. X-ray diffraction of the ZnO seeds, before and after calcination. ZnO: zinc oxide.

The NO_3^- produces the following reaction



The presence of Zn^{2+} causes consumption of the OH^- ions generated in the electrode, by generating ZnO precipitation.²⁹

The cyclic voltammetry (Figure 1(a)) shows a peak of reduction of the hydroxide precursor that can be O_2 or NO_3^- at -0.85 V and another at -1.1 V that is due to the formation of ZnO on the electrode surface.

In the electrochemical deposition of the Ag nanoparticles, the formation of a crystalline structure with spherical morphology is observed and this is due to the use of surfactant (PVP).

Organic encapsulating reagents such as PVP are used for the selective synthesis of metallic nanoparticles due to their ability to affect their growth by a selective adhesion to specific crystalline planes.³⁰

The structural shape in the deposition of Ag can be modified by two variables: the current density “ J ” and the molar ratio R

$$R = \frac{n_{\text{PVP}}}{\text{Ag}} (\text{monomer})$$

Each variable was analyzed and it was found that a high current density produces Ag in branched form (dendrites), while low current densities give agglomerates of compact nanoparticles. This effect is very similar to changing the intensity of a reducing agent in chemical reduction systems, where spherical nanoparticles are formed with a weak reducer, while dendrites are produced in the presence of strong reducers.³⁰

X-ray diffraction results for the ZnO samples electrodeposited by chronoamperometry, present peaks at 20.37° and 34.18° (Figure 4), corresponding to the (003) and (004) planes, respectively, of basic zinc acetate $(\text{Zn}_5(\text{OH})_8(\text{CH}_3\text{COO})_2 \cdot 2\text{H}_2\text{O})$.³¹ After calcination, these two peaks disappear, and the peaks corresponding to the (100), (002), and (101) planes of ZnO increase.

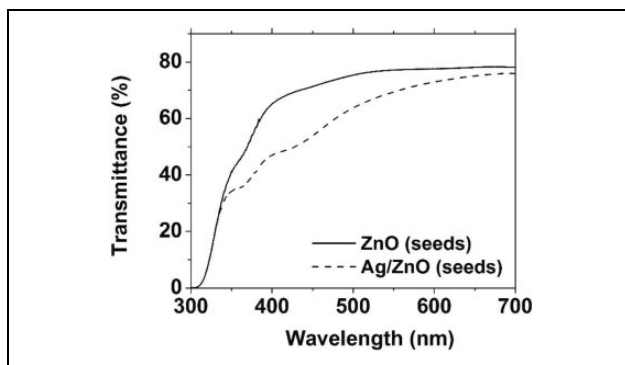


Figure 5. Optical transmittance between 300 nm and 700 nm of the ZnO (solid line) and Ag/ZnO (dashed line) seeds. ZnO: zinc oxide; Ag: silver.

Calcination changed the ratio of the sizes of the (002) and (101) peaks: the (101) peak is larger before calcination, while the (002) peak is larger afterward. It appears therefore that after electrodeposition of the seeds, a phase composed of ZnO and basic zinc acetate is obtained first, leaving only ZnO after calcination.

Optical transmittance of the seed samples in the 300–700 nm range is shown in Figure 5. The ZnO absorption peak, as well as the plasmon absorption peak at 450 nm, can be observed only in Ag/ZnO samples. Optical transmittance reduction in the visible range for the Ag/ZnO sample can be associated with metallic reflection from the deposited Ag seeds.

The growth of ZnO nanorods films on Ag/ZnO and ZnO seeds was studied with SEM (Figure 6). It can be seen that ZnO seeds formed initially as nanosheets (Figure 6(a)). After the 380°C heat treatment, these structures collapsed to form semispherical nanoparticles (Figure 6(b)) with a mean size of 21 nm.

The Ag/ZnO sample treated at 160°C (Figure 6(d)) showed spherical nanoparticles of 52.5 nm mean size. In the case of electrostatically deposited nanoparticles, the current density was very low (approximately $100 \mu\text{A}/\text{cm}^2$), which explains the spherical and compact shape of the Ag nanoparticles (Figure 6(d)). Very low concentrations of Ag (2×10^{-4} M) were used, which with respect to the relation R indicates us that with higher values there is a tendency to form smaller spherical structures $R > 100$.³⁰ Calculated value of R in our synthesis gives a value of approximately 180, which supports the hypothesis of the form obtained with the electrodeposition of Ag.

The the reduction of the Ag associated diffraction peak occurs because the ZnO seed films are porous- (Figure 6(b)). For the adhesion of the nanoparticles of Ag on that surface, was used electrodeposition at -0.4 V, and the film was formed with the characteristic (yellowish) coloration of the nanoparticles of Ag.

The ZnO nanorods films can be seen in Figure 6(c) and (e). There is a clear difference between the ZnO nanorods grown on Ag/ZnO seeds and those grown on ZnO seeds, as

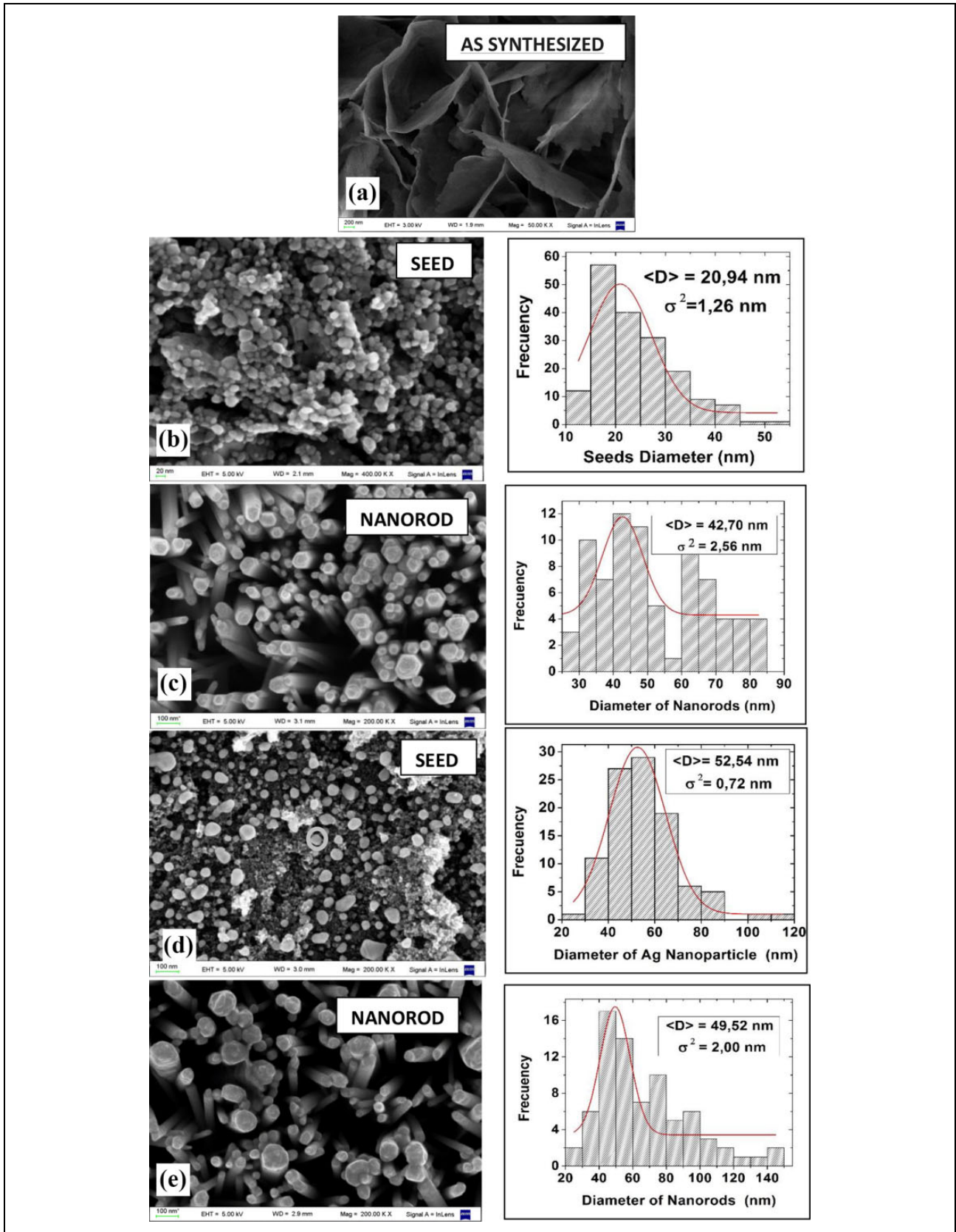


Figure 6. SEM images of (a) the electrodeposited ZnO seeds before and (b) after calcination, (c) ZnO nanorods obtained on the ZnO seeds, (d) Ag nanoparticles electrodeposited on calcinated ZnO seeds, and (e) ZnO nanorods obtained on Ag/ZnO seeds. Insets to the right shown the ZnO nanorod diameter distribution. SEM: scanning electron microscope; ZnO: zinc oxide; Ag: silver.

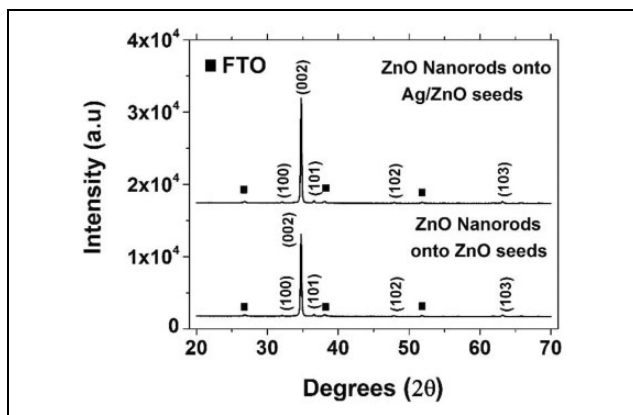


Figure 7. X-ray diffraction of ZnO nanorods. ZnO: zinc oxide.

the former are circular and the latter hexagonal in shape. This difference is attributable to the epitaxial growth typical of each film: the cubic structure of Ag nanoparticle seeds transforms the hexagonal structure of the ZnO nanorods to produce cylindrical nanorods.³² Conversely, ZnO seeds produce hexagonal nanorods, typical of the ZnO structure.

X-ray diffraction of the ZnO nanorods formed on Ag/ZnO and ZnO (Figure 7) showed the (100), (002), and (101) planes typical of the Wurtzite structure. The (002) preferential plane is characteristic of the orientation of the nanorods along the *c*-axis of the crystal structure.³³

It can be seen that Ag nanoparticles produce a preferential orientation along the (002) plane during the growth

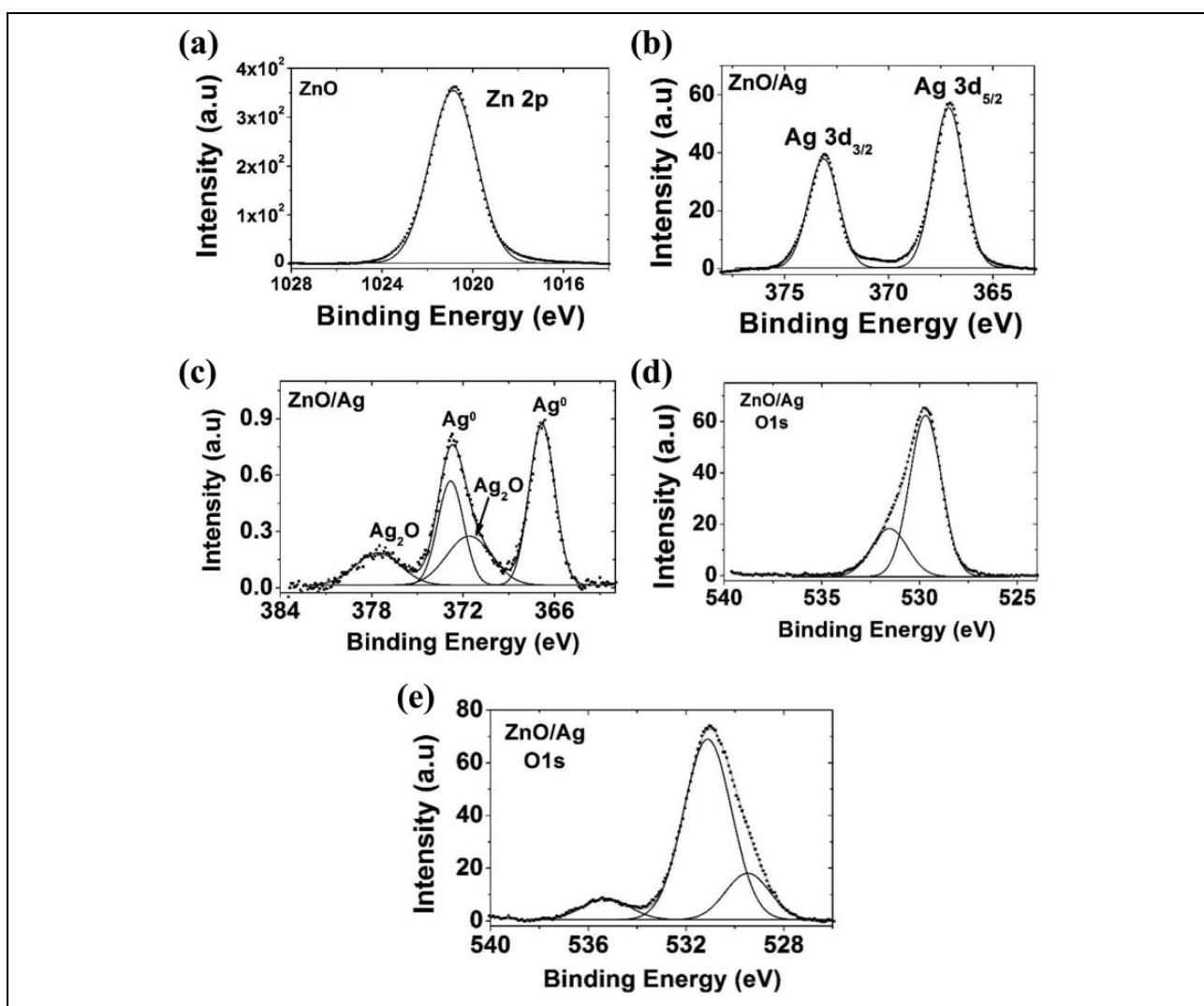


Figure 8. XPS spectra for (a) Zn 2p in the ZnO electrodeposited seeds, (b) Ag 3d in the Ag nanoparticles electrodeposited on ZnO seeds, (c) Ag 3d in the nanorods grown on Ag/ZnO seeds, (d) O 1s in the Ag/ZnO seeds, and (e) O 1s in the nanorods grown on Ag/ZnO seeds. XPS: X-ray photoelectron spectrophotometer; ZnO: zinc oxide; Ag: silver.

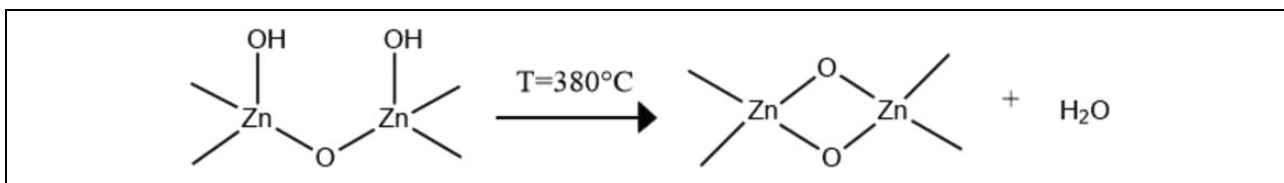


Figure 9. Formation of structural oxygen from superficial hydroxyls.³⁷

of the nanorods; small amounts of Ag are known to promote a growth effect along the *c*-axis of ZnO films³⁴

The XPS spectra give information on the elements present in the ZnO/Ag film and their chemical bonds in each phase of the growth process. Figure 8(a) shows the spectrum obtained for Zn in electrodeposited ZnO seeds after calcination, with the Zn 2p peak at 1020.8 eV, corresponding to Zn (II) in the ZnO structure.³⁵

The XPS spectrum for Ag 3d in the seeds (Figure 8(b)) presents two peaks for Ag (0) at 367.1 and 373.1 eV. As for the finished films containing nanorods, Figure 8(c) shows the spectrum of Ag 3d with two peaks at 366.81 and 372.81 eV, characteristic of the Ag (0) state.³⁶ It also shows two supplementary peaks at 371.59 and 377.59 eV, indicating the formation of a silver oxide (Ag₂O) layer³⁶ during the growth of the ZnO nanorods on these nanoparticles.

One can observe that the intensity of the Ag 3d XPS spectra is larger for the ZnO seeds with Ag nanoparticles than for the finished film of ZnO nanorods grown on the same seeds. This can be explained by the method of analysis, which is superficial; the Ag nanoparticles are more easily detected when they are present on the ZnO seeds than when the ZnO nanorods have grown on the surface.

The O₂ XPS spectrum of the ZnO seeds (Figure 8(d)) shows two types of O₂ bonds: a higher 529.7 eV peak corresponding to the ZnO structural oxygen³⁷ (O²⁻) and a smaller 531.5 eV peak corresponding to the O₂ of the superficial hydroxyls³⁷ (-OH) bonded to the ZnO species. These features are obtained because the 380°C heat treatment has caused desorption of most of the superficial hydroxyls to form water and the structure outlined in Figure 9.

Unlike the ZnO seeds, the nanorods have an O₂ XPS spectrum (Figure 8(e)), where the main peak (531.1 eV) corresponds to the O₂ of the superficial hydroxyls, and the smaller peak (529.5 eV) to the structural O₂. This is the reverse of what was observed for the ZnO seeds, since the nanorods were formed at 90°C, and at this temperature, the dehydration of the hydroxyls does not take place and the surface of the nanorods contains therefore more -OH. A smaller peak at 535.3 eV may be due to chemisorbed water on the surface of the nanorods.

The illumination of a film of ZnO nanorods without Ag produces a change in current, due to the light-induced photocurrent on the semiconductor (Figure 3(a)). An increase in the photocurrent was also observed for the ZnO films containing Ag nanoparticles, as can be seen in

Figure 3(b), together with a comparison between this effect on ZnO films with or without Ag nanoparticles.

The influence of the nanoparticles in the production of photocurrent is due to the reflective effect of Ag nanoparticles when the beam of light hits the Ag/ZnO films. This effect can also be observed on the measurements of UV-Vis transmittance (Figure 5). The Ag nanoparticles caused a larger and different dispersion of light on the surface of the nanorods, compared to the samples without Ag, in such a way that the former absorbed a larger proportion of the light and produced a higher photocurrent.

Conclusions

A method has been developed for the synthesis of ZnO nanorods with Ag nanoparticle seeds, using the techniques of electrodeposition and chemical bath. A change in the structure of the seeds was obtained through heat treatment, transforming a mixture of ZnO and basic zinc acetate into pure ZnO, as evidenced by X-ray diffraction. The presence of Ag nanoparticles on the ZnO seeds caused a change in the morphology of the film, from the hexagonal-shaped nanorods characteristic of the ZnO seeds, to cylindrical-shaped nanorods on the Ag/ZnO seeds.

The plasmon absorption of ZnO/Ag seeds can produce a reflective effect to improve the light absorption in the nanorods of ZnO as a consequence the photocurrent increased.

The characteristics of the superficial atomic bonds of the films were obtained from the XPS spectra. The growth of the ZnO nanorods introduced changes on the surface of the Ag nanoparticles, with the appearance of peaks indicating to a thin layer of Ag₂O.

The O₂ XPS spectra revealed that the heat treatment of the sample resulted in a larger presence of interstitial O₂, compared to hydroxyl O₂, in the ZnO seeds. However, the ZnO nanorods showed a larger presence of hydroxyl O₂, compared to interstitial O₂, as their synthesis took place at only 90°C.

At potentials larger than 0.5 V, a larger photocurrent was observed on the ZnO nanorods grown on Ag/ZnO seeds, compared to those grown on ZnO seeds. This difference is attributed to the beneficial effect of Ag seeds, which reflect the light not absorbed by the sample and increase the photogeneration of the charge carriers.

Acknowledgments

Alejandro Aranda would like to thank the Peruvian Council for Science and Technology (CONCYTEC) for the Scholarship. Roberto Candal and Patricio Carnelli are members of CONICET.



Declaration of conflicting interests

The author(s) declared no potential conflicts of interest with respect to the research, authorship, and/or publication of this article.

Funding

The author(s) disclosed receipt of the following financial support for the research, authorship, and/or publication of this article: This work was supported by the project no. 133-FINCYT-IB-2015 and no. 113-INNOVATE PERU-ISASS-2018. This work is partially supported by PICT 2014 2386.

ORCID iD

Patricio Carnelli  <https://orcid.org/0000-0001-9874-550X>
 Juan Rodríguez  <https://orcid.org/0000-0002-9887-6419>

References

- Balkus KJ. *Metal oxide nanotube, nanorod, and quantum dot photocatalysis*. Amsterdam: Elsevier B.V, 2013. DOI: 10.1016/B978-0-444-53874-1.00009-3.
- Sharma S, Vyas S, Periasamy C, et al. Structural and optical characterization of ZnO thin films for optoelectronic device applications by RF sputtering technique. *Superlattice Microst* 2014; 75: 378–389. DOI: 10.1016/j.spmi.2014.07.032.
- Usha K, Mondal B, Sengupta D, et al. Development of multi-layered nanocrystalline TiO₂ thin films for photovoltaic application. *Opt Mater (Amst)* 2014; 36: 1070–1075. DOI: 10.1016/j.optmat.2014.01.037.
- Bahnemann D. Photocatalytic water treatment: solar energy applications. *Sol Energy* 2004; 77: 445–459. DOI: 10.1016/j.solener.2004.03.031.
- Kim ES, Hwang G, Gamal El-Din M, et al. Development of nanosilver and multi-walled carbon nanotubes thin-film nanocomposite membrane for enhanced water treatment. *J Memb Sci* 2012; 394–395: 37–48. DOI: 10.1016/j.memsci.2011.11.041.
- Lv J, Gong W, Huang K, et al. Effect of annealing temperature on photocatalytic activity of ZnO thin films prepared by sol-gel method. *Superlattice Microst* 2011; 50: 98–106. DOI: 10.1016/j.spmi.2011.05.003.
- Kaneva N, Bojinova A, Papazova K, et al. Effect of thickness on the photocatalytic properties of ZnO thin films. *Bulg Chem Commun* 2015; 47: 395–401.
- Wellings JS, Chaure NB, Heavens SN, et al. Growth and characterisation of electrodeposited ZnO thin films. *Thin Solid Films* 2008; 516: 3893–3898. DOI: 10.1016/j.tsf.2007.07.156.
- Kaneva NV, Dimitrov DT and Dushkin CD. Effect of nickel doping on the photocatalytic activity of ZnO thin films under UV and visible light. *Appl Surf Sci* 2011; 257: 8113–8120. DOI: 10.1016/j.apsusc.2011.04.119.
- Gonzalez-Valls I and Lira-Cantu M. Vertically-aligned nanostructures of ZnO for excitonic solar cells: a review. *Energy Environ Sci* 2009; 2: 19–34. DOI: 10.1039/b811536b.
- Al-Gaashani R, Radiman S, Daud AR, et al. XPS and optical studies of different morphologies of ZnO nanostructures prepared by microwave methods. *Ceram Int* 2013; 39: 2283–2292. DOI: 10.1016/j.ceramint.2012.08.075.
- Prete P, Lovergine N and Tapfer L. Nanostructure size evolution during Au-catalysed growth by carbo-thermal evaporation of well-aligned ZnO nanowires on (100)Si. *Appl Phys A Mater Sci Process* 2007; 88: 21–26. DOI: 10.1007/s00339-007-3946-4.
- Du LX, Wang KG, Hu XY, et al. Control of morphologies and properties of zinc oxide nanorod arrays by slightly adjusting their seed layers. *Nanomater Nanotechnol* 2016; 6: 1–8. DOI: 10.1177/1847980416663674.
- Singh S, Kumar Y, Kumar H, et al. A study of hydrothermally grown ZnO nanorod-based metal-semiconductor-metal UV detectors on glass substrates. *Nanomater Nanotechnol* 2017; 7: 1–5. DOI: 10.1177/1847980417702144.
- Thanh Son N, Noh J and Park S. Role of ZnO thin film in the vertically aligned growth of ZnO nanorods by chemical bath deposition. *Appl Surf Sci* 2016; 379: 440–445. DOI: 10.1016/j.apsusc.2016.04.107.
- Ren C, Yang B, Wu M, et al. Synthesis of Ag/ZnO nanorods array with enhanced photocatalytic performance. *J Hazard Mater* 2010; 182: 123–129. DOI: 10.1016/j.jhazmat.2010.05.141.
- Chu D, Masuda Y, Ohji T, et al. Formation and photocatalytic application of ZnO nanotubes using aqueous solution. *Langmuir* 2010; 26: 2811–2815. DOI: 10.1021/la902866a.
- Pauporte T and Rathousky J. Electrodeposited mesoporous ZnO thin films as efficient photocatalysts for the degradation of dye pollutants. *J Phys Chem C* 2007; 111: 7639–7644.
- Sathishkumar P, Sweena R, Wu JJ, et al. Synthesis of CuO-ZnO nanophotocatalyst for visible light assisted degradation of a textile dye in aqueous solution. *Chem Eng J* 2011; 171: 136–140. DOI: 10.1016/j.cej.2011.03.074.
- Kumar R, Singh AP, Thakur P, et al. Ferromagnetism and metal-semiconducting transition in Fe-doped ZnO thin films. *J Phys D Appl Phys* 2008; 41: 155002. DOI: 10.1088/0022-3727/41/15/155002.
- Gacic M, Jakob G, Herbert C, et al. Magnetism of co-doped ZnO thin films. *Phys Rev B* 2007; 75: 205206(1–8). DOI: 10.1103/PhysRevB.75.205206.
- Rai P, Kim Y, Song H, et al. Chemical the role of gold catalyst on the sensing behavior of ZnO nanorods for CO and NO₂ gases. *Sensors and Actuators B Chem* 2012; 165: 133–142. DOI: 10.1016/j.snb.2012.02.030.
- Zeng H, Cai W, Liu P, et al. ZnO-based hollow nanoparticles by selective etching: elimination and reconstruction of metal-semiconductor interface, improvement of blue emission and photocatalysis. *ACS Nano* 2008; 2: 1661–1670.
- Rashid J, Barakat MA, Salah N, et al. Ag/ZnO nanoparticles thin films as visible light photocatalysts. *RSC Adv* 2014; 4: 56892–56899. DOI: 10.1039/C4RA12990C.

25. Yang J, Liu X and Du X. Electrodeposition of silver nanoparticles on ITO films with different thickness and application as LSPR sensor, ECS electrochem. *Lett* 2014; 3: B30–B32. DOI: 10.1149/2.0061412eel.
26. Berruet M and Vázquez M. Electrodeposition of single and duplex layers of ZnO with different morphologies and electrical properties. *Mater Sci Semicond Process* 2010; 13: 239–244. DOI: 10.1016/j.mssp.2010.08.001.
27. Bian J, Li Z, Chen Z, et al. Electrodeposition of silver nanoparticle arrays on ITO coated glass and their application as reproducible surface-enhanced Raman scattering substrate. *Appl Surf Sci* 2011; 258: 1831–1835. DOI: 10.1016/j.apsusc.2011.10.055.
28. Rodríguez J, Paraguay-Delgado F, López A, et al. Synthesis and characterization of ZnO nanorod films for photocatalytic disinfection of contaminated water. *Thin Solid Films* 2010; 519: 729–735. DOI: 10.1016/j.tsf.2010.08.139.
29. Skompska M and Zarębska K. Electrodeposition of ZnO nanorod arrays on transparent conducting substrates – a review. *Electrochim Acta* 2014; 127: 467–488. DOI: 10.1016/j.electacta.2014.02.049.
30. Meng XK, Tang SC and Vongehr S. Invited review a review on diverse silver nanostructures. *J Mater Sci Technol* 2010; 26: 487–522. DOI: 10.1016/S1005-0302(10)60078-3.
31. Cui Q, Yu K, Zhang N, et al. Porous ZnO nanobelts evolved from layered basic zinc acetate nanobelts. *Appl Surf Sci* 2008; 254: 3517–3521. DOI: 10.1016/j.apsusc.2007.11.044.
32. Liu X, Li F, Wang Y, et al. Surface-enhanced Raman scattering and photocurrent multiplication phenomenon of ZnO/Ag nanoarrays. *Mater Lett* 2013; 94: 19–22. DOI:10.1016/j.matlet.2012.11.128.
33. Sima M and Vasile E. Preparation of nanostructured ZnO nanorods in a hydrothermal-electrochemical process. *Thin Solid Films* 2012; 520: 4632–4636. DOI: 10.1016/j.tsf.2011.10.116.
34. Karyaoui M, Mhamdi A, Kaouach H, et al. Some physical investigations on silver-doped ZnO sprayed thin films. *Mater Sci Semicond Process* 2015; 30: 255–262. DOI: 10.1016/j.mssp.2014.09.017.
35. Zhang L, Zhao J, Lu H, et al. Facile synthesis and ultrahigh ethanol response of hierarchically porous ZnO nanosheets. *Sensors Actuators, B Chem* 2012; 161: 209–215. DOI: 10.1016/j.snb.2011.10.021.
36. Xu C, Tian M, Liu L, et al. Fabrication and properties of silverized glass fiber by dopamine functionalization and electroless plating. *J Electrochem Soc* 2012; 159: 217–224. DOI: 10.1149/2.056204jes.
37. Khajavi MR, Blackwood DJ, Cabanero G, et al. New insight into growth mechanism of ZnO nanowires electrodeposited from nitrate-based solutions. *Electrochim Acta* 2012; 69: 181–189. DOI: 10.1016/j.electacta.2012.02.096.